INDUCTION COUPLING BETWEEN JOINTLESS TRACK CIRCUITS AND TRACK-CIRCUIT-READER ANTENNA

Lin-Hai Zhao[*] and Wei-Shi Shi

School of Electronics and Information Engineering, Beijing Jiaotong University, Beijing 100044, China

Abstract—This paper presents herein experiments and calculations of electromagnetic induction between jointless track circuits (JTCs) and track-circuit readers (TCRs). The paper uses transmission-line theory to simulate JTC currents ahead of shunt points and electromagnetism to calculate voltages induced in the TCR antenna. Based on these calculations, the JTC-to-TCR range is defined. The paper derives expressions for the amplitude and phase of the voltage induced in the TCR antenna by the JTC current and uses them to quantitatively analyze the train control system. Experiments verify the conclusions reached based on the calculations.

1. INTRODUCTION

Jointless track circuits (JTCs) are a key component of train control systems (TCSs) and are used for train detection. Through electromagnetic induction, JTC currents in the rails can induce voltages in track-circuit-reader (TCR) antennae, enabling continuous transmission of train control information.

Currently, with the rapid development of high-speed railways, train operations demand an ever-higher level of speed control. Therefore, the track-train continuous information transmission process (TTCITP) between JTCs and TCRs, which transfers information about reliability and safety, must be fully adapted to the requirements of high-speed railways. To do this, TTCITP theory must be perfected to provide the basis for further research into the reliability and safety of TCSs. However, because development of high-speed railways is at different stages around the world, the railway devices and operating

conditions differ; hence, the TTCITP does not attract sufficient theoretical attention. To date, most research focuses either on JTCs or TCRs separately.

For JTC, models of rail impedance and adjacent track interference were based on the finite element method [1, 2]. In [3], the JTC-signal frequency and phase were designed. In [4], distributive track-circuit parameters were calculated using a semidiagonal matrix of finite elements. In [5], a track circuit was digitally simulated via boundary-condition analysis, and the adaptability of ballastless track circuits was studied in [6]. Moreover, we have presented a model of the normal-state rail-surface voltage and that of the short-circuit current of the leading wheels and axle of the locomotive in the shunted state [7, 8]. We also systematically analyzed the influence on the JTC of compensation capacitors, ballast resistance, and transmitter voltage [9]. For TCR, the magnetic-field distribution of an infinite-length direct-current circuit was used to develop a static model of electromagnetic induction by the track-circuit current of voltage in the TCR antenna [10]. Finally, we used transmission-line theory to study the transmission of voltage induced on TCR antenna to the host computer [11].

This brief review of previous research shows that previous studies of JTC and TCR do not analyze JTC and TCR as a whole system but rather model the individual devices. Although research on electromagnetic induction from JTC to TCR is available in [10], the main problems studied treat the track circuit as a direct-current circuit of infinite length and neglect the ballast resistance and compensation capacitors. Such an approach is inconsistent with real operating conditions, physical structures, and signal-transformation processes; therefore, the conclusions of the research require experimental verification. Furthermore, the voltage induced in the TCR antenna is generally considered to be linear in the short-circuit current of the leading wheels and axle of the locomotive [12, 13] and to depend on the track-circuit-signal carrier frequencies [14]. However, to date, no theoretical formula explains this linear relationship; therefore, it is difficult to ascertain the linear relationship parameters. This paper addresses these shortfalls by studying the entire JTC and TCR together.

The paper is organized as follows: Section 2 briefly introduces the work principle and the structures of JTC and TCR. Section 3 introduces the dynamic JTC signal current model. Section 4 introduces the model of the JTC-TCR electromagnetic-induction process. Section 5 analyzes the amplitude and phase of the voltage induced in the TCR antenna, the JTC current, and the relationship

between the two. Section 6 presents experiments that verify the calculated results for amplitude and phase. Finally, Section 7 concludes the paper.

2. WORK PRINCIPLE AND STRUCTURES OF JTC AND TCR

As shown in Figure 1, JTCs consist essentially of a transmitter, a transmitting cable, transmitting electrical tuning units, track lines with two rails and equal-spaced compensation capacitors, receiving electrical tuning units, a receiving cable, and a receiver. The TCR is an onboard device that consists of TCR antennae, TCR transmission cable, and TCR host computer.
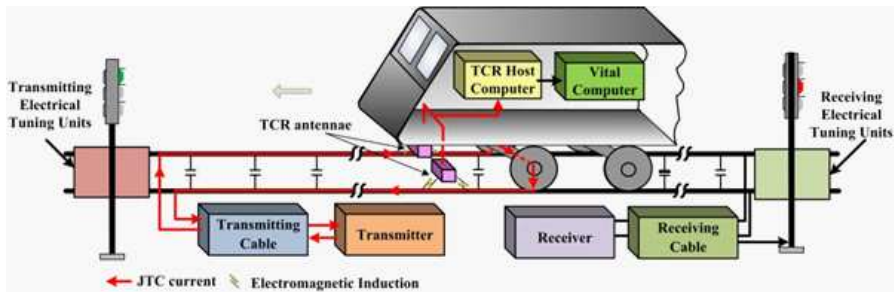
Figure 1. Basic structure and working principle of JTC and TCR.

According to installation specifications [12], one TCR antenna is installed ahead of the leading locomotive wheels and over each rail. As shown in Figure 2, the two antennae are perpendicular to their respective rail. The performance and internal structure of the two antennae are identical; both comprise an iron core about which two independent coils are wound. In a given antenna, each coil is in series with a similarly positioned coil from the other antenna to make a diploid redundant structure, which improves the reliability of the TCR antennae.

To control train speed and detect train occupancy, the transmitter generates a JTC signal containing train target speed. The signal goes through the transmitting cable, transmitting electronic tuning units and then through the rails into the receiving end of JTC. The JTC signal $U_f(t)$ generated by the transmitter is [13, 14]

$$U_f(t) = A_f \cos[\omega(t) + \phi_0], \quad \omega(t) = 2\pi f_c t + 2\pi \Delta f_p \int s_m(t) dt, \quad (1)$$
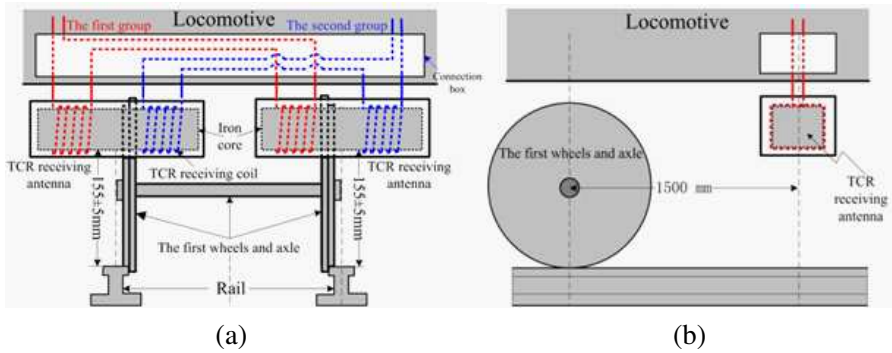
Figure 2. Basic structure and position of TCR antennae. (a) Front view. (b) Side view.

where A_f, f_c, Δf_p, and ϕ_0 are the amplitude, carrier frequency, frequency offset, and initial JTC-signal phase, respectively. The quantity $s_m(t)$ is a 50% duty cycle square-wave signal of frequency f_d corresponding to a specific train target speed. Table 1 details the frequency parameters of JTC signal.

Table 1. Frequency parameters of JTC signal.

JTC Type		ZPW-2000A JTC				Domestic frequency-shift JTC	
f_c (Hz)	Up-train direction	2001.4	1998.7	2601.4	2598.7	650	850
	Down-train direction	1701.4	1698.7	2301.4	2298.7	550	750
Δf_p (Hz)		±11				±55	
f_d (Hz)		$10.3 + 1.1 \times n$, $n = 0 \sim 17$				7,8,8.5,9,9.5,11, 12,12.5,13.5,15,16, 16.5,17.5,18.5,20, 22.5,23.5,24.5,26	

When a train enters a track circuit, the JTC signal is shunted by the leading wheels and axle of the locomotive, following which most of the JTC signal flows back into the transmitter with only a small portion entering the receiver. Simultaneously, voltage is induced electromagnetically in the TCR antenna by the JTC and then transmitted into the TCR host computer through the TCR

transmission cable. The train target speed is obtained by demodulation and decoding in the TCR host computer and then transmitted to the vital computer for train control.

3. MODEL OF JTC CURRENT IN SHUNTED STATE

To study the relationship between the JTC current and voltage induced in the TCR antenna, we model and analyze the distribution of JTC current ahead of the leading wheels and axle of the locomotive. Let the near end of the transmitting units be the origin point o. The JTC current $I_d(x, x_1, t)$ of every point $x_1 \in [0, x]$ is modeled by transmission line theory [15] (Figure 3).
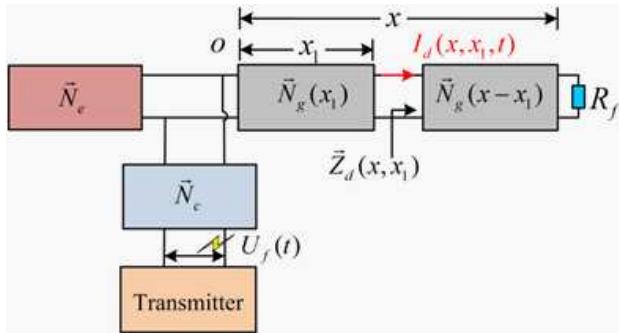
Figure 3. Distribution model of JTC current in shunted state.

R_f is the equivalent shunt resistance of the train, $\vec{N}_c$ and $\vec{N}_e$ are the equivalent four-terminal networks (EFTNs) of the transmitting cable and transmitting electronic tuning units, respectively. $\vec{N}_g(x_1)$ and $\vec{N}_g(x - x_1)$ are the EFTNs for the track lines from o to x_1 and x_1 to x, respectively. With the shunt point at x, $\vec{Z}_d(x, x_1)$ is the apparent impedance from x_1 to the receiving end and $I_d(x, x_1, t)$ is the JTC current at x_1.

According to Figure 3 and Eq. (1), $I_d(x, x_1, t)$ is

$$I_d(x, x_1, t) = A_d(x, x_1) \cos[\omega(t) + \phi_d(x, x_1)]. \tag{2}$$

Here, $A_d(x, x_1)$ and $\phi_d(x, x_1)$ denote the amplitude and phase of $I_d(x, x_1, t)$, respectively, and are given as [16]

$$A_d(x, x_1) = A_f \left/ \left| \vec{N}_{s11}(x_1) \vec{Z}_d(x, x_1) + \vec{N}_{s12}(x_1) \right| \right.,$$

$$\phi_d(x, x_1) = \phi_0 - \arg \left[\vec{N}_{s11}(x_1) \vec{Z}_d(x, x_1) + \vec{N}_{s12}(x_1) \right], \tag{3}$$

where $|\cdot|$ is the complex modulus operator, $\vec{N}_{s11}(x_1)$ and $\vec{N}_{s12}(x_1)$ are the characteristic parameters of $\vec{N}_s(x_1)$, and $\vec{N}_s(x_1)$ is the overall EFTN of devices from the transmitting cable to x_1. $\vec{N}_s(x_1)$ must satisfy

$$\vec{N}_s(x_1) = \begin{bmatrix} \vec{N}_{s11}(x_1) & \vec{N}_{s12}(x_1) \\ \vec{N}_{s21}(x_1) & \vec{N}_{s22}(x_1) \end{bmatrix} = \vec{N}_c \times \vec{N}_e \times \vec{N}_g(x_1), \qquad (4)$$

where $\vec{N}_g(x_1)$ is the EFTN of track lines from x_1 to o and is

$$\vec{N}_g(x_1) = \begin{bmatrix} \vec{N}_{g11}(x_1) & \vec{N}_{g12}(x_1) \\ \vec{N}_{g21}(x_1) & \vec{N}_{g22}(x_1) \end{bmatrix} = \left(\vec{N}_t\right)^{k_1} \times \vec{N}_y(x_1, k_1 l_T/2). \qquad (5)$$

Here, $\vec{N}_t$ is the EFTN of a compensation unit, which consists of a compensation capacitor C and two track lines of length $l_T/2$, which is half the distance between adjacent compensation capacitors. If $\vec{N}_{cp}$ and $\vec{N}_{gg}(l_T/2)$ are the EFTNs of the compensation capacitor C and the track lines of length $l_T/2$, respectively, then

$$\vec{N}_t = \begin{bmatrix} \vec{N}_{t11} & \vec{N}_{t12} \\ \vec{N}_{t21} & \vec{N}_{t22} \end{bmatrix} = \vec{N}_{gg}(l_T/2) \times \vec{N}_{cp} \times \vec{N}_{gg}(l_T/2), \quad (6)$$

$$\vec{N}_{gg}(l_T/2) = \begin{bmatrix} \cosh\left(\vec{\gamma}_g \cdot l_T/2\right) & \vec{z}_g \sinh\left(\vec{\gamma}_g \cdot l_T/2\right) \\ \sinh\left(\vec{\gamma}_g \cdot l_T/2\right)/\vec{z}_g & \cosh\left(\vec{\gamma}_g \cdot l_T/2\right) \end{bmatrix}. \qquad (7)$$

If $\vec{z}_g$ and $\vec{\gamma}_g$ are the impedance and propagation constant of the rails, respectively, then $\vec{z}_d$ and $\vec{\gamma}_d$ are the impedance of the rail and ballast resistance [8, 11], respectively, and are given by [17]

$$\vec{z}_g = \sqrt{\vec{z}_d \vec{\gamma}_d}, \quad \vec{\gamma}_g = \sqrt{\vec{z}_d/\vec{\gamma}_d}. \qquad (8)$$

If k_1 is the number of complete compensation units in the track lines from o to x_1, then $\vec{N}_y(x_1, k_1 l_T/2)$ is the EFTN of the remaining part (which cannot constitute a complete compensation unit) of the track lines from o to x_1, except for the k_1 complete compensation units. $\vec{N}_y(x_1, k_1 l_T/2)$ is given by

$$\vec{N}_y(x_1, k_1 l_T/2) = \begin{cases} \vec{N}_{gg}(x_1 - k_1 l_T/2), \\ k_1 l_T/2 \le x_1 < (k_1 + 1)l_T/2 \\ \vec{N}_{gg}(x_T/2) \times \vec{N}_{cp} \times \vec{N}_{gg}[x_1 - (k_1 + 1)l_T/2], \\ (K_1 + 1)l_T/2 \le x_1 < (k_1 + 2)l_T/2, \end{cases} \qquad (9)$$

and $\vec{Z}_d(x, x_1)$ is [18–20]

$$\vec{Z}_d(x, x_1)$$
$$= \left(\vec{N}_{g11}(x - x_1)R_f + \vec{N}_{g12}(x - x_1)\right) \Big/ \left(\vec{N}_{g21}(x - x_1)R_f + \vec{N}_{g22}(x - x_1)\right), (10)$$

where $\vec{N}_{g11}(x - x_1)$ and $\vec{N}_{g12}(x - x_1)$ are the characteristic parameters of $\vec{N}_g(x - x_1)$, which is the EFTN of the track lines from x_1 to x and satisfies

$$\vec{N}_g(x - x_1) = \begin{bmatrix} \vec{N}_{g11}(x - x_1) & \vec{N}_{g12}(x - x_1) \\ \vec{N}_{g21}(x - x_1) & \vec{N}_{g22}(x - x_1) \end{bmatrix}$$
$$= \vec{N}_y(x_1, k_1 l_T/2)^{-1} \times \left(\vec{N}_t \right)^{k_2+1}, \qquad (11)$$

where k_2 is the number of the complete compensation units in the track lines from x_1 to x.

According to Eqs. (3)–(11), $A_d(x, x_1)$ and $\phi_d(x, x_1)$ can be simulated when the shunt point is the entry point ($x = l_g$, where l_g is the total JTC length) and the JTC midpoint ($x = l_g/2$), respectively (Figure 4). According to the JTC adjustment sheet [21], the corresponding simulation settings are $l_g = 960\,\mathrm{m}$, $f_c = 2601.4\,\mathrm{Hz}$, $A_f = 78\,\mathrm{V}$, $r_d = 3\,\Omega \cdot \mathrm{km}$, $R_f = 0.25\,\Omega$, and the total number of compensation capacitors in one JTC is $k = 12$.

Figure 4 shows that overall, $A_d(x, x_1)$ and $\phi_d(x, x_1)$ both gradually increase from the receiving to the transmitting end of the JTC. The detailed variations of $A_d(x, x_1)$ and $\phi_d(x, x_1)$ depend on the locations of the compensation capacitors; between two adjacent compensation capacitors, the variations of $A_d(x, x_1)$ and $\phi_d(x, x_1)$ are small and relatively stable. However, $A_d(x, x_1)$ and $\phi_d(x, x_1)$ both use the compensation capacitors as demarcation points; hence, on each side of the compensation capacitors $A_d(x, x_1)$ oscillates stepwise and $\phi_d(x, x_1)$ gradually increases stepwise. In addition, $A_d(x, x_1)$ and $\phi_d(x, x_1)$ depend similarly on the shunt point x; namely $A_d(x, x_1)$, $x_1 \in [0, C6]$ and $A_d(x, x_1)$, $x_1 \in [C6, C12]$, and $\phi_d(x, x_1)$, $x_1 \in [0, C6]$ and $\phi_d(x, x_1)$, $x_1 \in [C6, C12]$ are essentially identical; the only difference
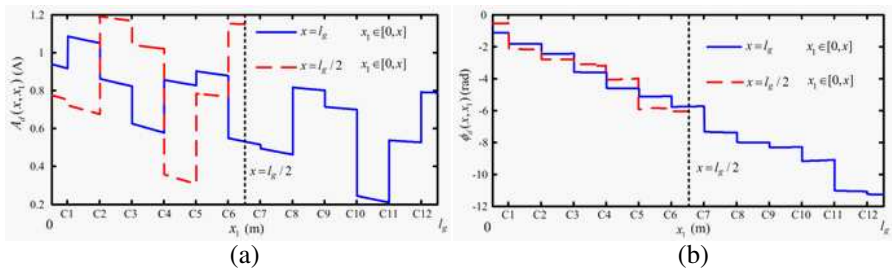
Figure 4. Simulation of (a) amplitude $A_d(x, x_1)$ and (b) phase $\phi_d(x, x_1)$ of $I_d(x, x_1, t)$, where $x = l_g$, $x = l_g/2$, $x_1 \in [0, x]$ with l_g being the total JTC length.

being that $A_d(x, x_1)$, $x_1 \in [0, C6]$ and $\phi_d(x, x_1)$, $x_1 \in [0, C6]$ are closer to the transmitting end of the track circuit and hence are greater than $A_d(x, x_1)$, $x_1 \in [C6, C12]$ and $\phi_d(x, x_1)$, $x_1 \in [C6, C12]$.

Note that the compensation capacitors, which are in parallel with the rails lines, cause $\vec{Z}_d(x, x_1)$, $\vec{N}_{s11}(x_1)$, and $\vec{N}_{s12}(x_1)$ to vary on each side; therefore, they directly affect the impedance-matching capability of the JTC, thereby causing large variations between the incident and reflected signals. When x_1 lies between two adjacent compensation capacitors, there are no compensation capacitors within in this region; hence, $\vec{Z}_d(x, x_1)$, $\vec{N}_{s11}(x_1)$, and $\vec{N}_{s12}(x_1)$ are smoother in this region.

4. MODEL OF ELECTROMAGNETIC INDUCTION BETWEEN JTC AND TCR

As discussed above, the compensation capacitors cause $A_d(x, x_1)$ and $\phi_d(x, x_1)$ between the shunt point x and the origin o to vary discontinuously, which differs from the original mechanical-insulation track circuit. Therefore, to study how the stepwise variation of the JTC current influences the voltage induced in the TCR antenna, we model the electromagnetic induction between the JTC and TCR. This mainly consists of calculating the magnetic flux in the TCR antenna, delimiting the region in which that JTC current mainly contributes to the induced voltage, and mathematically describing the voltage induced in the TCR antenna.

4.1. Calculation of Magnetic Flux in TCR Antenna

As shown in Figure 5, we take O to be the origin of a Cartesian coordinate system. The dimensions of the TCR antenna are $ab = 2l_b$, $ad = 2l_a$, and $ag = 2l_c$, the widths of the coils are l_q, the number of turns is q_m, the distance from the iron-core center to the inner edge of the coils is l_p, the height from the lower edge of the iron core to the rail surface is l_h, the horizontal distance from the leading-wheel axle center to the TCR antenna center is l_m, and $e(x_0, y_0, z_0)$ is an arbitrary point on the TCR-antenna induction coils.

The Biot-Savart law [22, 23] gives the magnetic-induction intensity B_e [24] generated by the JTC current in the rails from x to x_1 ($x_1 \in [0, x]$) at the arbitrary point $e(x_0, y_0, z_0)$ as

$$B_e(x, x_1, t, x_0, y_0, z_0) = \frac{\mu_0 \mu_r}{4\pi} \int_{x_1}^{x} I_d(x, x', t) \left(y_0^2 + z_0^2\right)^{1/2}$$
$$\left(\sqrt{(|x_0 - x'|)^2 + y_0^2 + z_0^2}\right)^{-3} dx', \quad (12)$$
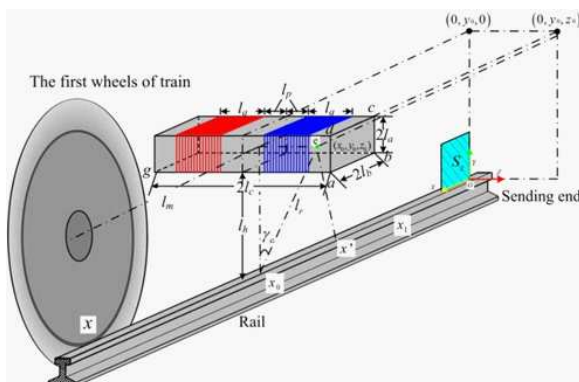
Figure 5. Coordinate system for TCR antenna, rails, and leading wheels.

where μ_0 is the permeability of vacuum and μ_r the relative permeability of the iron core. The corresponding magnetic flux $\Phi_e(x, x_1, z_0, t)$ of S_z is [25]

$$\Phi_e(x, x_1, z_0, t) = \frac{q_m}{l_q} \int\limits_{l_h}^{l_h+2l_a} \int\limits_{x-l_m-l_b}^{x-l_m+l_b} B_e(x, x_1, t, x_0, y_0, z_0)$$

$$y_0 \left(y_0^2 + z_0^2\right)^{-1/2} dx_0 dy_0. \tag{13}$$

Let the total magnetic flux in each induction coil of a TCR antenna be $\Phi_1(x, x_1, t)$ and $\Phi_2(x, x_1, t)$, where

$$\Phi_1(x, x_1, t) = \Phi_{11}(x, x_1, t) - \Phi_{12}(x, x_1, t) = \Phi_2(x, x_1, t)$$
$$= \Phi_{22}(x, x_1, t) - \Phi_{21}(x, x_1, t), \tag{14}$$

with $\Phi_{11}(x, x_1, t)$ and $\Phi_{22}(x, x_1, t)$ being the total self-magnetic flux of each induction coil in a TCR antenna. According to Eq. (13), they can be expressed as [25]

$$\Phi_{11}(x, x_1, t) = \Phi_{22}(x, x_1, t) = \int_{l_p}^{l_p+l_q} \Phi_e(x, x_1, z_0, t) dz_0. \tag{15}$$

The fluxes $\Phi_{12}(x, x_1, t)$ and $\Phi_{21}(x, x_1, t)$ are the mutual magnetic fluxes of the two induction coils in one TCR antenna and can be expressed as [25]

$$\Phi_{12}(x, x_1, t) = \Phi_{21}(x, x_1, t) = I_c(x, x_1, t) M_c, \tag{16}$$

where $I_c(x, x_1, t)$ is the self-inductance current in the coils:

$$I_c(x, x_1, t) = \frac{1}{z_c} \frac{d\Phi_{11}(x, x_1, t)}{dt}. \tag{17}$$

In Eq. (17), $\vec{z}_c$ is the impedance of one coil and M_c (H) the mutual-induction coefficient of the two coils in one TCR antenna [26, 27]:

$$M_c = \int_{l_p}^{l_p+l_q} \int_{l_h}^{l_h+2l_a} \int_{x-l_m-l_b}^{x-l_m+l_b} [M_{ab}(x_0, y_0, z_0) + M_{bc}(x_0, y_0, z_0)$$
$$+ M_{cd}(x_0, y_0, z_0) + M_{da}(x_0, y_0, z_0)]dx_0 dy_0 dz_0, \qquad (18)$$

where $M_{ab}(x_0, y_0, z_0)$, $M_{bc}(x_0, y_0, z_0)$, $M_{cd}(x_0, y_0, z_0)$, and $M_{da}(x_0, y_0, z_0)$ (H/m^3) are the magnetic-induction coefficients at the arbitrary point $e(x_0, y_0, z_0)$ in one coil in the directions ab, bc, cd, and da. These coefficients connect the self-inductance current $I_c(x, x_1, t)$ of the other coil of the same TCR antenna (Figure 6). They are given by

$$M_{ab}(x_0, y_0, z_0) = \frac{q_m \mu_0 \mu_r}{4\pi(z_0 + l_p)} \left(\frac{e_1' a_1}{ea_2} - \frac{e_1' b_1}{eb_2} \right),$$

$$M_{bc}(x_0, y_0, z_0) = \frac{q_m \mu_0 \mu_r}{4\pi(z_0 + l_p)} \left(\frac{e_2' b_1}{eb_2} - \frac{e_2' c_1}{ec_2} \right),$$

$$\qquad (19)$$

$$M_{cd}(x_0, y_0, z_0) = \frac{q_m \mu_0 \mu_r}{4\pi(z_0 + l_p)} \left(\frac{e_3' c_1}{ec_2} - \frac{e_3' d_1}{ed_2} \right),$$

$$M_{da}(x_0, y_0, z_0) = \frac{q_m \mu_0 \mu_r}{4\pi(z_0 + l_p)} \left(\frac{e_4' d_1}{ed_2} - \frac{e_4' a_1}{ea_2} \right),$$

where ea_2, eb_2, ec_2, and ed_2 are the distances from $e(x_0, y_0, z_0)$ in one coil to a_2, b_2, c_2, and d_2 in the other coil of the same TCR antenna, respectively. They are given by

$$ea_2 = \sqrt{(x_0 - x + l_m - l_b)^2 + (y_0 - l_h)^2 + (z_0 + l_p)^2},$$

$$ec_2 = \sqrt{(x_0 - x + l_m + l_b)^2 + (y_0 - l_h - 2l_a)^2 + (z_0 + l_p)^2},$$

$$\qquad (20)$$

$$eb_2 = \sqrt{(x_0 - x + l_m + l_b)^2 + (y_0 - l_h)^2 + (z_0 + l_p)^2},$$

$$ed_2 = \sqrt{(x_0 - x + l_m - l_b)^2 + (y_0 - l_h - 2l_a)^2 + (z_0 + l_p)^2}.$$

e_1', e_2', e_3', and e_4' are the perpendicular points of $e(x_0, y_0, z_0)$ in the directions of ab, bc, cd, and da, respectively. The quantities a_1, b_1, c_1, and d_1 are located in the same coil as e, and $e_1' a$, $e_1' b$, $e_2' b$, $e_2' c$, $e_3' c$, $e_3' d$, $e_4' d$ and $e_4' a$ are the distances from e_1' to a, e_1' to b, e_2' to b, e_2' to c, e_3' to c, e_3' to d, e_4' to d, and e_4' to a, respectively. They satisfy

$$e_1' a = e_3' d = |x_0 - x + l_m - l_b|, \quad e_2' b = e_4' a = |y_0 - l_h|,$$
$$e_1' b = e_3' c = |x_0 - x + l_m + l_b|, \quad e_2' c = e_4' d = |y_0 - l_h - 2l_a|.$$

$$\qquad (21)$$
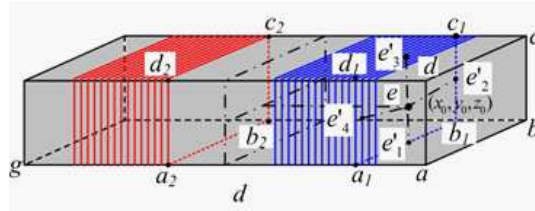
Figure 6. Coordinate system of TCR antenna.

4.2. Delimiting JTC-to-TCR Range

Based on the discussion above, the magnetic flux in the TCR antenna generated by the JTC currents in the track lines from x to o can be calculated using Eqs. (12)–(21). Because the JTC current ahead of the shunt point fluctuates stepwise, with the compensation capacitors serving as demarcation points, the JTC-to-TCR range (in which the JTC current contributes the most to the induced voltage) must be determined to simplify the calculation of the electromagnetic induction between the JTC and the TCR antenna. This range can be determined by calculating the contribution to the magnetic flux in the TCR antenna by the JTC current from every point in the track lines ahead of the shunt point x.

Based on the simulation settings given for Figure 4 and using Eqs. (12)–(21), the total magnetic flux $\Phi_1(x, x_1, t)$, $x_1 \in [0, x]$ in the TCR-antenna induction coils is calculated for several shunt points. The simulation step is $\Delta x = 0.001\,\text{m}$, the number of simulation steps is $j = 0, 1, \ldots, \lfloor x/\Delta x \rfloor$, where

$$x_1 = x - j\Delta x. \tag{22}$$

Figure 7 shows the simulation result. We find that the JTC-to-TCR range is independent of the shunt points and that the flux contribution
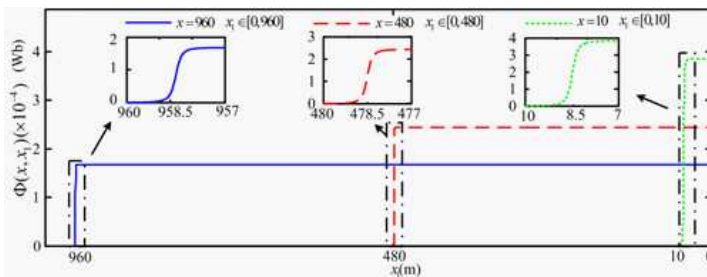
Figure 7. Simulation of $\Phi(x, x_1, t)(x = 960,\ x = 480,\ x = 10)$.

is approximately the same from the origin to the shunt point as from three meters before the shunt point to the shunt point. Thus,

$$\Phi_1(x, x_1, t), \quad x \in [0, x] \approx \Phi_1(x, x_1, t), \quad x_1 \in [x - 3, x]. \tag{23}$$

We also analyze the contribution of the current at each point in the JTC-to-TCR range to the magnetic flux at the TCR antenna. The magnetic flux at the TCR antenna is

$$\Delta\Phi_1(x, j, t) = \Phi_1[x, x - (j+1)\Delta x, t] - \Phi_1(x, x - j\Delta x, t),$$
$$j = 0, 1, 2, \ldots, \lfloor(3 - \Delta x)/\Delta x\rfloor, \quad x \in [0, l_g]. \tag{24}$$

Figure 8 shows the flux change $\Delta\Phi_1(x, j, t)$ between each simulation step $[x-(j+1)\Delta x, x-j\Delta x], j = 0, 1, 2, \ldots, [(3-\Delta x)/\Delta x], x \in [0, l_g]$.

Figure 8 shows that the maximum magnetic flux at the TCR antenna is generated by the JTC current at a point 1.5 m before the shunt point; namely

$$\Delta\Phi_1(x, \lfloor(1.5)/\Delta x\rfloor, t) = \max(\Delta\Phi_1(x, j, t)),$$
$$j = 0, 1, 2, \ldots, \lfloor(3 - \Delta x)/\Delta x\rfloor, \quad x \in [0, l_g]. \tag{25}$$

The distance of 1.5 m is not only half of the JTC-to-TCR range, but also the location of the TCR antenna center.
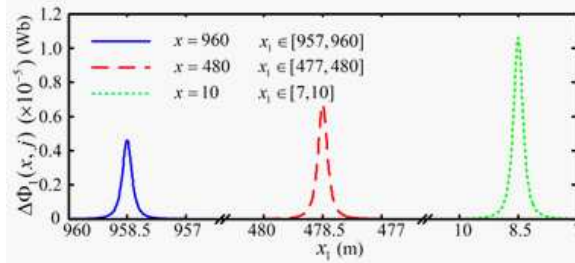
Figure 8. Simulation of $\Delta\Phi_1(x, j, t)$ ($x = 960$, $x = 480$, $x = 10$).

4.3. Model of Voltage Induced in TCR Antenna

Based on the above conclusions and the Faraday law of electromagnetic induction [28], the induced voltages $\varepsilon_1(x)$ and $\varepsilon_2(x)$ generated in the two sets of induction coils in a pair of TCR antennae are equal and can be expressed as

$$\varepsilon_1(x) = \varepsilon_2(x) = -\frac{2d\Phi_1(x, x - 3, t)}{dt} = -\frac{2d\Phi_2(x, x - 3, t)}{dt}. \tag{26}$$

According to Eqs. (14)–(17) and (26), $\varepsilon_1(x)$ and $\varepsilon_2(x)$ can be rewritten as

$$\varepsilon_1(x) = \varepsilon_2(x) = -2 \left(\frac{d\Phi_{11}(x, x-3, t)}{dt} + \frac{M_c}{\vec{z}_d} \frac{d^2\Phi_{11}(x, x-3, t)}{dt^2} \right)$$

$$= -2 \left(\frac{d\Phi_{22}(x, x-3, t)}{dt} + \frac{M_c}{\vec{z}_d} \frac{d^2\Phi_{22}(x, x-3, t)}{dt^2} \right). \tag{27}$$

Here supposes a integral function $F[f_{un}(\cdot)]$ as:

$$F[f_{un}(\cdot)] = \int_{l_p}^{l_p+l_q} \int_{l_h}^{l_h+2l_a} \int_{x-l_m-l_b}^{x-l_m+l_b}$$

$$\left[\int_{x-3}^{x} f_{un}(\cdot) y_0 \left[\sqrt{(|x_0-x'|)^2 + y_0^2 + z_0^2} \right]^{-3} dx' \right] dx_0 dy_0 dz_0 \tag{28}$$

From Eqs. (2), (12), (13), (15), and (27), we find

$$\varepsilon_1(x) = \varepsilon_2(x) = F\left[a_{k_1} I_{k_1}\left(x, x', t\right)\right] + F\left[a_{k_2} I_{k_2}\left(x, x', t\right)\right], \tag{29}$$

where

$$I_{k_1}(x, x', t) = A_d(x, x') \sin\left[\omega(t) + \phi_d\left(x, x'\right)\right],$$
$$a_{k_1} = \mu_0 \mu_r q_m [f_c + \Delta f_p s_m(t)]/l_q,$$
$$I_{k_2}(x, x', t) = A_d(x, x') \cos\left[\omega(t) + \phi_d\left(x, x'\right)\right], \tag{30}$$
$$a_{k_2} = 2\pi \mu_0 \mu_r q_m M_c [f_c + \Delta f_p s_m(t)]^2 / \vec{z}_c l_q,$$

Note that a_{k_1} and a_{k_2} are both approximately constant because f_c, Δf_p, and $s_m(t)$ (the parameters of the JTC signal; Table 1) and μ_0, μ_r, q_m, l_q, l_p, l_h, l_a, l_m, l_b, and $\vec{z}_c$ are all constants, known, and can be obtained from the inward structure and installation standard of the TCR antenna [12]. Furthermore, $I_{k_1}(x, x', t)$ and $I_{k_2}(x, x', t)$ can be written as

$$I_{k_1}(x, x', t) = A_d(x, x') \cos[\phi_d(x, x')] \sin[\omega(t)]$$
$$+ A_d(x, x') \sin[\phi_d(x, x')] \cos[\omega(t)],$$
$$I_{k_2}(x, x', t) = A_d(x, x') \cos[\phi_d(x, x')] \cos[\omega(t)] \tag{31}$$
$$- A_d(x, x') \sin[\phi_d(x, x')] \sin[\omega(t)].$$

Substituting Eq. (31) into Eq. (29), we find

$$\varepsilon_1(x) = \varepsilon_2(x) = a_{\varepsilon 1}(x) \sin[\omega(t)] + a_{\varepsilon 2}(x) \cos[\omega(t)], \tag{32}$$

where

$$a_{\varepsilon 1}(x) = F[A_d(x, x') a_{k_1} \cos(\phi_d(x, x'))]$$
$$- F[A_d(x, x') a_{k_2} \sin(\phi_d(x, x'))],$$
$$a_{\varepsilon 2}(x) = F[A_d(x, x') a_{k_1} \sin(\phi_d(x, x'))] \tag{33}$$
$$+ F[A_d(x, x') a_{k_2} \cos(\phi_d(x, x'))],$$

If there exists a phase function $\phi_\varepsilon(x)$ satisfying

$$\cos[\phi_\varepsilon(x)] = a_{\varepsilon 1}(x)/\sqrt{a_{\varepsilon 1}(x)^2 + a_{\varepsilon 2}(x)^2},$$
$$\sin[\phi_\varepsilon(x)] = a_{\varepsilon 2}(x)/\sqrt{a_{\varepsilon 1}(x)^2 + a_{\varepsilon 2}(x)^2}, \tag{34}$$

then inserting Eqs. (32) and (33) into Eq. (31) gives

$$\varepsilon_1(x) = \varepsilon_2(x) = A_\varepsilon(x) \sin\{[\omega(t)] + \phi_\varepsilon(x)\}, \tag{35}$$

where $A_\varepsilon(x)$ and $\phi_\varepsilon(x)$ are the amplitude and phase of $\varepsilon_1(x)$ and $\varepsilon_2(x)$, respectively, and are given by

$$A_\varepsilon(x) = \sqrt{a_{\varepsilon 1}(x)^2 + a_{\varepsilon 2}(x)^2}, \quad \phi_\varepsilon(x) = \text{angle}\,[a_{\varepsilon 1}(x) + i a_{\varepsilon 2}(x)]. \tag{36}$$

The operator angle$(\cdot)$ is the complex phase operator and i is the imaginary unit of complex.

5. DEPENDENCE OF VOLTAGE INDUCED IN TCR ANTENNA ON AMPLITUDE AND PHASE OF JTC CURRENT

Comparison of Eqs. (35) and (2) reveals that although electromagnetic induction between the JTC and TCR may change the corresponding amplitude and phase, the parameters f_c, Δf_p, and f_d, remain unchanged. Therefore, we analyze the electromagnetic induction between the JTC and TCR from the viewpoints of amplitude and phase.

5.1. Simulation of Voltage Amplitude and Phase Induced in TCR Antenna by JTC Current

Based on the simulation settings used for Figure 4 and according to Eqs. (3) and (36), we simulate the amplitude $A_\varepsilon(x)$ and phase $\phi_\varepsilon(x)$, respectively, of the voltage induced in the TCR antenna, the amplitude $A_d(x, x - l_m)$ and phase $\phi_d(x, x - l_m)$ of the JTC current beneath the center of the TCR antenna, and the amplitude $A_d(x, x)$ and phase $\phi_d(x, x)$ of the short-circuit current flowing through the leading wheels and axle of the locomotive. The results of the simulation are shown in Figures 9 and 10.

5.2. Relationship between Voltage Amplitude and Phase Induced in TCR Antenna by JTC Current

5.2.1. No Compensation Capacitors in JTC-to-TCR Range

The results shown in Figures 9 and 10 indicate that when there are no compensation capacitors in the JTC-to-TCR range,

$$A_d(x, x) \approx A_d(x, x - l_m), \quad \phi_d(x, x) \approx \phi_d(x, x - l_m), \tag{37}$$
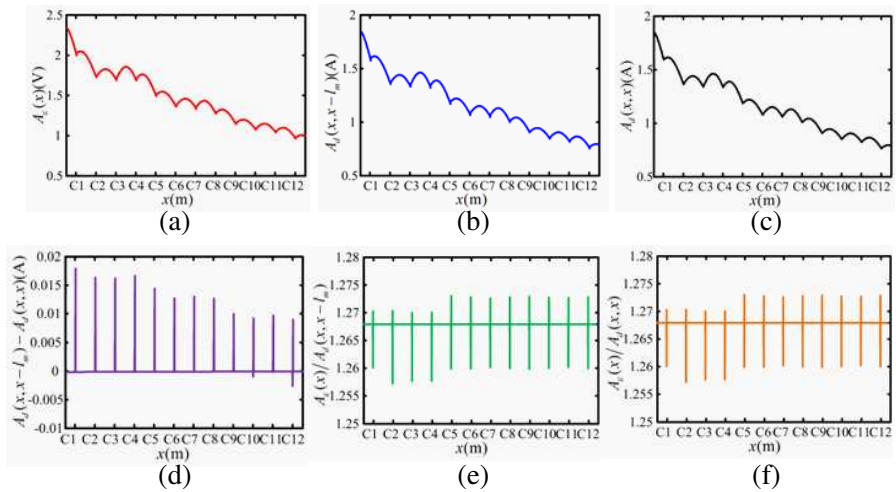
Figure 9. Results of simulation of (a) $A_\varepsilon(x)$, (b) $A_d(x, x - l_m)$, (c) $A_d(x, x)$, (d) $A_d(x, x - l_m) - A_d(x, x)$, (e) ratio of $A_\varepsilon(x)$ to $A_d(x, x - l_m)$ and (f) ratio of $A_\varepsilon(x)$ to $A_d(x, x)$.
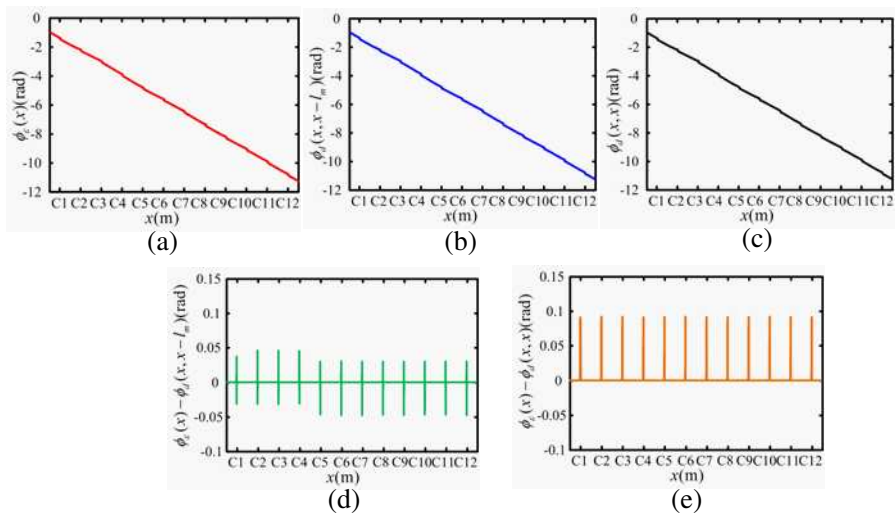
Figure 10. Results of simulation of (a) $\phi_\varepsilon(x)$, (b) $\phi_d(x, x - l_m)$, (c) $\phi_d(x, x)$, (d) error between $\phi_\varepsilon(x)$ and $\phi_d(x, x - l_m)$, and (e) error between $\phi_\varepsilon(x)$ and $\phi_d(x, x)$.

Eq. (37) can be understood by considering the attenuation constant α and phase-shift constant β of the JTC. These constants refer to the amplitude attenuation and phase delay of the JTC signal per unit length of rail, respectively, and can be expressed by the rail propagation constant $\vec{\gamma}_g$ [Eq. (8)]; namely, $\alpha = \text{real}(\vec{\gamma}_g)$ and $\beta = \text{Im}(\vec{\gamma}_g)$ [29, 30]. From the parameters of the JTC devices [12], we know that the amplitude attenuation and phase delay of the JTC signal after flowing through 3 m of rail are small ($\sim 10^{-3}$). From Eq. (25), $A_d(x, x')$ and $\phi_d(x, x')$ are approximately equivalent in the range $x' \in [x - 3, x]$:

$$\begin{cases} A_d\left(x, x'\right) \approx A_d\left(x, x - l_m\right) \\ \phi_d\left(x, x'\right) \approx \phi_d\left(x, x - l_m\right) \end{cases} \quad x' \in [x - 3, x], \tag{38}$$

Substituting Eq. (38) in Eq. (33), Eq. (35) takes the form

$$\varepsilon_1(x) = \varepsilon_2(x) = k_\varepsilon \sqrt{a_{k_1}^2 + a_{k_2}^2} A_d(x, x - l_m) \cos\{[\omega(t)] + \phi_\varepsilon'(x)\}, \tag{39}$$

where

$$\begin{aligned} k_\varepsilon &= F[f_{un}(\cdot) = 1], \tag{40} \\ \phi_\varepsilon' &= -\pi/2 + \text{angle}\{[a_{k_1}\cos(x, x - l_m) - a_{k_2}\sin(x, x - l_m)] \\ &\quad + i[a_{k_1}\sin(x, x - l_m) + a_{k_2}\cos(x, x - l_m)]\}. \tag{41} \end{aligned}$$

If we suppose

$$\sin(\phi_k) = a_{k_2}/\sqrt{a_{k_1}^2 + a_{k_2}^2}, \qquad \cos(\phi_k) = a_{k_1}/\sqrt{a_{k_1}^2 + a_{k_2}^2}, \tag{42}$$

then Eq. (41) gives

$$\begin{aligned} \phi_\varepsilon'(x) &= -\pi/2 + \phi_d(x, x - l_m) + \phi_k, \tag{43} \\ \phi_k &= \text{angle}(a_{k_1} + ia_{k_2}). \tag{44} \end{aligned}$$

From Eqs. (30) and (39), k_ε and ϕ_k are constant, and owing to the TCR antenna structure, the induction coefficient M_c is relatively small and the impedance $\vec{z}_c$ of the coil is relative large; thus, Eq. (44) implies

$$a_{k_1} \gg a_{k_2}. \tag{45}$$

Therefore, Eq. (44) becomes

$$\phi_k \approx 0. \tag{46}$$

Defining a_1 as the ratio of $A_\varepsilon(x)$ to $A_d(x, x - l_m)$ and using Eq. (41), a_1 can be written as

$$\begin{aligned} a_1 &= A_\varepsilon(x)/A_d(x, x - l_m) = k_\varepsilon \sqrt{a_{k_1}^2 + a_{k_2}^2} \approx k_\varepsilon a_{k_1} \\ &= k_\varepsilon \mu_0 \mu_r q_m [f_c + \Delta f_p s_m(t)]/l_q, \tag{47} \end{aligned}$$

because μ_0, μ_r, q_m, l_q, and k_ε are constant. For a given JTC, f_c and Δf_p are constant from when a train enters the JTC to when it leaves the JTC. According to Eqs. (39) and (2), the phase difference $\Delta\phi_d(x)$ between the voltage induced in the TCR antenna and the JTC current is

$$\Delta\phi_d(x) = \phi'_\varepsilon(x) - \phi_d(x, x - l_m) \approx -\pi/2. \qquad (48)$$

For a given JTC, Eqs. (38), (47), and (48) indicate that with no compensation capacitors in the JTC-to-TCR range, the amplitude of JTC current is equivalent to that of the short-circuit current, and the voltage amplitude in the TCR antenna is linear in the JTC current, whereas the phases differs by about $-\pi/2$.

5.2.2. Compensation Capacitors in JTC-to-TCR Range

Figures 9 and 10 show that $A_d(x, x')$ and $\phi_d(x, x')$ vary around the compensation capacitors if these are present in the JTC-to-TCR range. Thus, we cannot simplify Eq. (36). However, the influence of this variation on a_1 and $\Delta\phi_d(x)$ is limited. Comparison of Eqs. (47) and (48) reveals that the maximum deviations of the amplitude and phase are 0.03% and 0.018%, respectively. With compensation capacitors in the JTC-to-TCR range, the amplitude of JTC current cannot be approximated as the short-circuit current. Only for cases that do not require high accuracy can the amplitude and phase be approximated by Eqs. (47) and (48).

6. EXPERIMENTAL VERIFICATION

6.1. Experimental Platform

Figure 11 shows the experimental platform, which mainly consists of a comprehensive tester, a transmission cable, ballast bed, two rails, an equivalent shunt resistance, two TCR antennae, two TCR receiving cable, a TCR host computer, and a TCR lamp. The comprehensive tester transmits many track circuit signals, including UM-71, ZPW-2000, and the domestic JTC frequency-shift signal (DFSS), and works with the TCR host computer to monitor the voltage induced in the TCR antenna. Here, the train shunt point is simulated by an equivalent resistance; therefore, the short-circuit current in the rails is acquired from the measured short-circuit voltage divided by the shunt resistance.
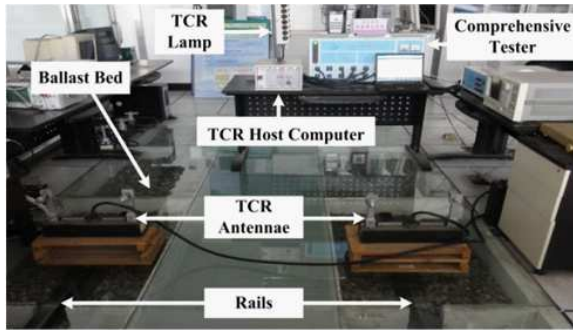
Figure 11. Experimental platform.
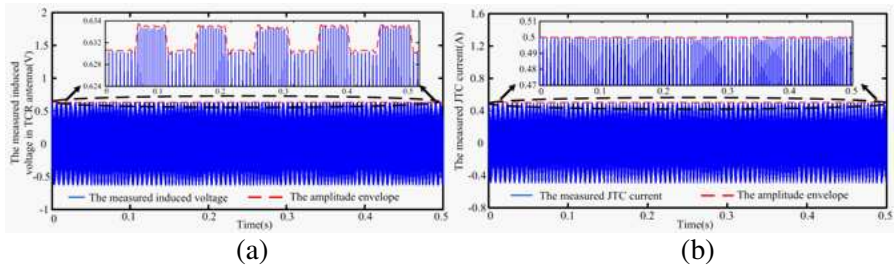
Figure 12. (a) Measured voltage induced in TCR antenna and (b) corresponding JTC current for ZPW2000A JTC.

6.2. Verification of Voltage Amplitude Induced in TCR Antenna by JTC Current and Their Linear Relationship

With the experimental platform, we measured the voltage induced in the TCR antenna and the JTC current for ZPW2000A-JTC used widely. Figure 12 shows the measured induced voltage and the corresponding measured JTC current and their amplitude envelopes. Figure 13 shows that the measured ratio $A_\varepsilon(x)$ to $A_d(x, x - l_m)$ agrees with the calculated ratio [Eq. (47)].

Figure 13 shows that the ratio of the measured amplitude of the induced voltage to the measured JTC current agrees with the ratio calculated using Eq. (47) This result means that Eq. (47) reflects the linear relationship between the voltage induced in the TCR antenna and JTC current.

Equation (47) also shows that the calculated ratio a_1 is related to Δf_p. For the ZPW2000A JTC, $\Delta f_p = 11\,\text{Hz}$ and $f_c = 1700\text{–}2600\,\text{Hz}$. Thus, $\Delta f_p \ll f_c$, so Δf_p only weakly influences the voltage induced in the TCR antenna, making it difficult to distinguish the high and
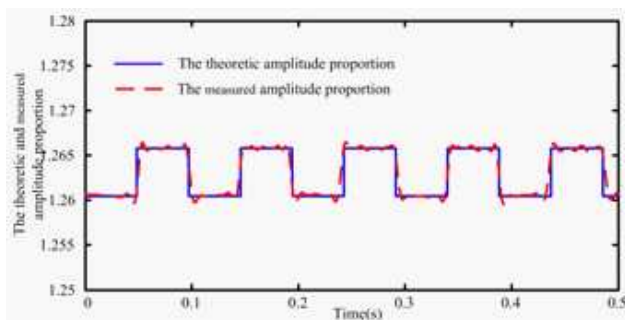
Figure 13. Measured amplitude ratio and that calculated using Eq. (47). Measured values are from Figure 12.
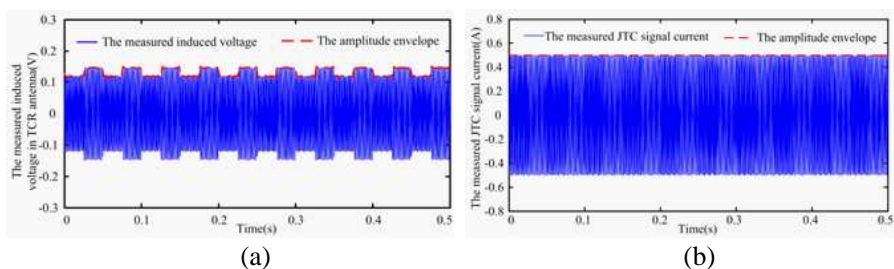
Figure 14. (a) Measured voltage induced in TCR antenna and (b) corresponding JTC current for DFSS JTC.

low side-band of the induced voltage [see Figure 12(a)] and verify the relationship given by Eq. (47) between a_1 and Δf_p. However, for the DFSS JTC, $\Delta f_p = 55\,\text{Hz}$ but f_c ranges only from 550 to 850 Hz, so the high and low side-band of the induced voltage are easily distinguished. In this work, we used the DFSS JTC to verify the theoretical relationship between a_1 and Δf_p.

Figure 14 shows the measured induced voltage and the corresponding measured JTC current for the DFSS JTC and their amplitude envelopes. The resulting amplitude ratio is compared to the ratio calculated using Eq. (47) in Figure 15.

From Figure 14(a), we can easily distinguish the high and low side-band of the induced voltage. Figure 15 shows that the measured amplitude ratio agrees with the ratio calculated with Eq. (47). This result indicates that Eq. (47) reflects the relationship between a_1 and Δf_p.

In conclusion, the voltage amplitude induced in the TCR antenna is linear in the JTC current, as expressed by Eq. (47).
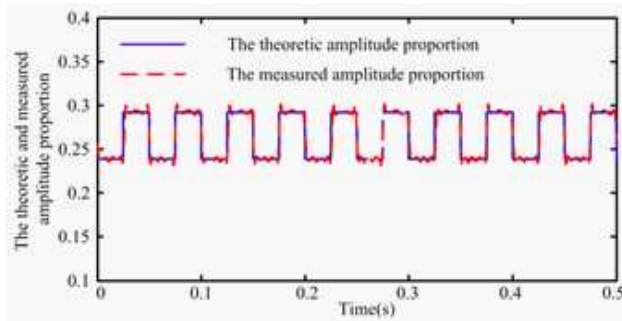
Figure 15. Measured amplitude ratio and that calculated using Eq. (47). Measured values are from Figure 14.

6.3. Verification of Phase between Voltage Induced in TCR Antenna and JTC Current

The voltage induced in the TCR antenna and JTC current for the ZPW2000A JTC were acquired to analyze their phases (Figure 16).

Figure 16 shows that the phase difference between the voltage induced in the TCR antenna and JTC current of the ZPW2000A JTC is about $-\pi/2$, which agrees with Eq. (48).
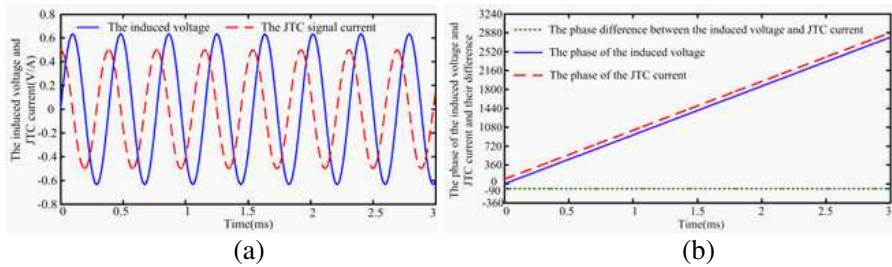
Figure 16. (a) Phase of voltage induced in TCR antenna and JTC current and (b) their phase difference.

7. STUDY OF THE INFLUENCE OF THE VELOCITY OF THE TUDY TRAIN

With the rapid development of high-speed railways, this paper takes into account the velocity of the train in the induction coupling between JTC and TCR antenna. Here supposes f_s as the sample frequency of the TCR host computer, m as the number of the total sampling points collected when the train passes through JTC, and $v(n)$ ($n = 1, 2, \ldots, m$) as the velocity of the train at each sampled time $t = n/f_s$

$(n = 1, 2, \ldots, m)$, then x can be expressed by

$$x = \sum_{j=1}^{n} v(j)/f_s, \quad (n = 1, 2, \ldots, m). \tag{49}$$

For simplicity, the paper focuses on the case that the train runs at a constant velocity, namely

$$v(1) = v(2) = \ldots = v(m) = v, \tag{50}$$

therefore, Eq. (49) can be rewritten as

$$x = vn/f_s = vt, \tag{51}$$

substituting Eq. (51) in Eq. (36), Eq. (36) takes the form

$$A_\varepsilon(vt) = \sqrt{a_{\varepsilon 1}(vt)^2 + a_{\varepsilon 2}(vt)^2}, \quad \phi_\varepsilon(vt) = \text{angle}\left[a_{\varepsilon 1}(vt) + i a_{\varepsilon 2}(vt)\right]. \tag{52}$$

Based on the simulation settings used for Figure 4 and according to Eq. (52), we simulate the amplitude $A_\varepsilon(vt)$ and phase $\phi_\varepsilon(vt)$ of the voltage induced in the TCR antenna respectively when $v = 240\,\text{km/h}$ and $360\,\text{km/h}$, and analyze $A_\varepsilon(vt)$ and $\phi_\varepsilon(vt)$ when the train passes through the same position ($x = 620\,(\text{m})$) of the same JTC with different velocities, as shown in Figure 17.

Figure 17 shows that when the train passes through the same position of the same JTC with different velocities, whatever the velocity of the train is, $A_\varepsilon(vt)$ and $\phi_\varepsilon(vt)$ remain unchanged. Namely, the velocity of the train has no influence on the amplitude and phase of the voltage induced in the TCR antenna. This can be explained by Eqs. (33) and (36), only $A_d(x, x')$ and $\phi_d(x, x')$ are related to the velocity of the train, and as known from Eqs. (3)–(11), for a given x in the same JTC, no matter what the velocity of the train is, the values of $A_d(x, x')$ and $\phi_d(x, x')$ are unchanged.

As to Eqs. (47) and (48), they are irrelevant to the variable x, namely the velocity of the train has no influence on the amplitude linearity and the phase difference $\pi/2$ between the voltage induced in the TCR antenna and JTC current.
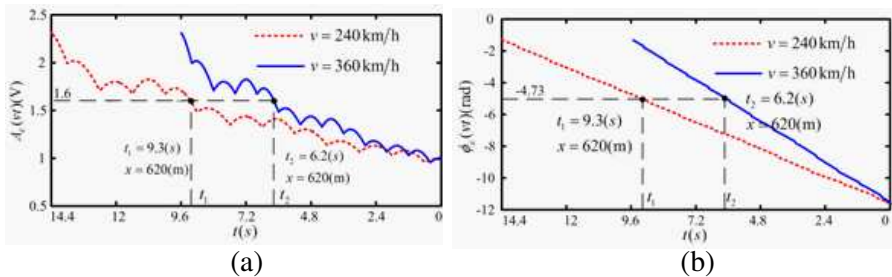
Figure 17. Results of simulation of (a) $A_\varepsilon(vt)$ and (b) $\phi_\varepsilon(vt)$, where $v = 240\,\text{km/h}$ and $360\,\text{km/h}$.

8. CONCLUSION

As key components of TCSs, the JTC and TCR transmit track-train control information by electromagnetic induction. This paper uses transmission line theory and electromagnetism to model the JTC current ahead of the shunt point and the voltage induced in the TCR antenna, respectively. Using this model, the paper quantitatively studies the relationship between the voltage induced in the TCR antenna and JTC current. The results indicate that the JTC-to-TCR range is about 3 m long and that within this range, the voltage amplitude induced in TCR antenna is linear in the JTC current and the phase difference is $\pi/2$, no matter what the velocity of the train is. The equations derived herein for the amplitude and phase of the voltage induced in the TCR antenna are verified experimentally and are more precise than the existing method based on the short-circuit current.

REFERENCES

1. Carpenter, D. C. and R. J. Hill, "Railroad track electrical impedance and adjacent track crosstalk modeling using the finite-element method of electromagnetic systems analysis," *IEEE Transactions on Vehicular Technology*, Vol. 42, No. 4, 555–562, 1993.

2. Hill, R. J. and D. C. Carpenter, "Rail track distributed transmission line impedance and admittance: Theoretical modelling and experimental results," *IEEE Transactions on Vehicular Technology*, Vol. 42, No. 4, 225–541, 1993.

3. Bebova, S., "Model of a laser-frequency measuring device," *IEEE International Symposium on Electronics*, 639–642, Pretoria, 1998.

4. Chen, Y. S. and L. A. Chen, "Semi diagonal matrix method of finite elements for calculation of track circuit," *Journal of the China Railway Soc.*, Vol. 21, No. 6, 54–57, 1999.

5. Zhao, H. B. and Y. Z. Zhang, "Study on some problems of track circuit with compensating capacitors," *Journal of the China Railway Soc.*, Vol. 20, No. 4, 77–81, 1998.

6. Gao, S. B., T. Tao, Z. Y. Hou, and Y. Ruan, "The adaptability analysis of jointless track circuit for ballastless track," *Electric Railway*, z1, 2006.

7. Zhao, L. H., Y. K. Ran, and J. C. Mu, "A comprehensive fault diagnosis method for jointless track circuit based on genetic algorithm," *China Railway Science*, Vol. 31, No. 3, 107–114, 2010.

8. Zhao, L. H. and J. C. Mu, "Fault diagnosis method for jointless track circuit based on AOK-TFR," *Journal of Southwest Jiaotong University*, Vol. 46, No. 1, 85–91, 2011.

9. Zhao, L. H., B. G. Cai, K. M. Qiu, and S. Q. Lv, "The method of diagnosis of compensation capacitor failures with jointless track circuits based on HHT and DBWT," *Journal of the China Railway Soc.*, Vol. 33, No. 3, 49–54, 2011.

10. Su, J., D. Y. Jiang, and P. X. Du, "The dynamic test method on track circuits," *Application of Electron Technique*, Vol. 32, No. 11, 7–10, 2006.

11. Zhao, L. H., J. P. Wu, and Y. K. Ran, "Fault diagnosis for track circuit using AOK-TFRs and AGA," *Control. Eng. Practice*, Vol. 20, No. 12, 1270–1280, 2012.

12. Qiu, K. M., *JT1-CZ2000 Type Cab Signal On-board System*, China Railway Press, Beijing, 2007.

13. Fei, X. K., *Principle and Analysis of Jointless Track Circuit*, China Railway Press, Beijing, 1993.

14. Bryleyev, A. M., *Analysis and Synthesis of Track Circuit*, China Railway Press, Beijing, 1981.

15. Liu, Y., L. Tong, W. H. Zhu, Y. Tian, and B. Gao, "Impedance measurements of nonuniform transmission lines in time domain using an improved recursive multiple reflection computation method," *Progress In Electromagnetics Research*, Vol. 117, 149–164, 2011.

16. Cao, W. Q., N. B. Zhang, J. A. Liu, B. T. Yu, S. D. Guo, and Y. Wei, "Novel phase-shifting characteristic of CRLH TL and its application in the design of dual-band dual-mode dual-polarization antenna," *Progress In Electromagnetics Research*, Vol. 131, 375–390, 2012.

17. Attiya, A. M., "Lower frequency limit of carbon nanotube antenna," *Progress In Electromagnetics Research*, Vol. 94, 419–433, 2009.

18. Torrungrueng, D. and S. Lamultree, "Equivalent graphical solutions of terminated conjugately characteristic impedance transmission lines with non-negative and corresponding negative characteristic resistances," *Progress In Electromagnetics Research*, Vol. 92, 137–151, 2009.

19. Lin, X. Q., P. Su, Y. Fan, and B. Z. Zhu, "Improved CRLH-TL with arbitrary characteristic impedance and its application in hybrid ring design," *Progress In Electromagnetics Research*, Vol. 124, 249–263, 2012.

20. Silapunt, R. and D. Torrrungruneng, "Theoretical study of microwave transistor amplifier design in the conjugately characteristic-impedance transmission line (CCITL) system using a bilinear transformation approach," *Progress In Electromagnetics Research*, Vol. 120, 309–226, 2011.

21. China Ministry of Railway, "General rules for China train control system technical specification," No. 14, 2004.

22. Wei, H. Y. and M. Soleimani, "Two-phase low conductivity flow imaging using magnetic induction tomography," *Progress In Electromagnetics Research*, Vol. 131, 99–115, 2012.

23. Kalhor, H. A., "The degree of intelligence of the law of Biot-Savart," *IEEE Transactions on Education*, Vol. 33, No. 4, 365–366, 1990.

24. Azpurua, M. A., "A semi-analytical method for the design of coil-systems for homogeneous magneto-static field generation," *Progress In Electromagnetics Research B*, Vol. 37, 171–189, 2012.

25. Cabanas, M. F., F. Pedrayes, M. G. Melero, C. H. Rojas, G. A. Orcajo, J. M. Cano, and J. G. Norniella, "Insulation fault diagnosis in high voltage power transformers by means of leakage flux analysis," *Progress In Electromagnetics Research*, Vol. 114, 211–234, 2011.

26. Ravaud, R., G. Lemarquand, and V. Lemarquand, "Mutual inductance and force exerted between thick coils," *Progress In Electromagnetics Research*, Vol. 102, 367–380, 2010.

27. Rui, C. M., "Mutual-inductance between two square loops with the same axis and size," *Journal of Wuhan Institute of Technology*, Vol. 29, No. 4, 90–92, 2007.

28. Witzel, J., "Faraday's law and nonconservative fields," *IEEE Instrumentation & Measurement Magazine*, Vol. 8, No. 1, 50–51, 2005.

29. Xie, H., J. Wang, R. Fan, and Y. Liu, "Study of loss effect of transmission lines and validity of a spice model in electromagnetic topology," *Progress In Electromagnetics Research*, Vol. 90, 89–103, 2009.

30. Eibert, T. F., Y. Weitsch, H. Chen, and E. M. Gruber, "Solving periodic eigenproblems by solving corresponding excitation problems in the domain of the eigenvalue," *Progress In Electromagnetics Research*, Vol. 126, 65–84, 2012.